

Eric Robalinho^{1*}, Edgar F. Cunha², Marcelo Linardi²

¹ Universidade Nove de Julho - UNINOVE, Rua Vergueiro, 235, São Paulo, Brasil

² IPEN/CNEN-SP, Av. Prof. Lineu Prestes, 2242, Cidade Universitária, São Paulo, Brasil

*e-mail: eric@ipen.br

Introduction: Two complementary 3D models were coupled to the overall modeling of PEM fuel cell. The modeling required multiphysics processes: gas flow at the distribution channels and porous media flow at GDL (model 1 – Entire Plate model); electrochemical reactions at catalyst layer and ionic charge transport at membrane (model 2 – MEA model). A schematic view of the regions where those phenomena occur is presented in Figure 1.

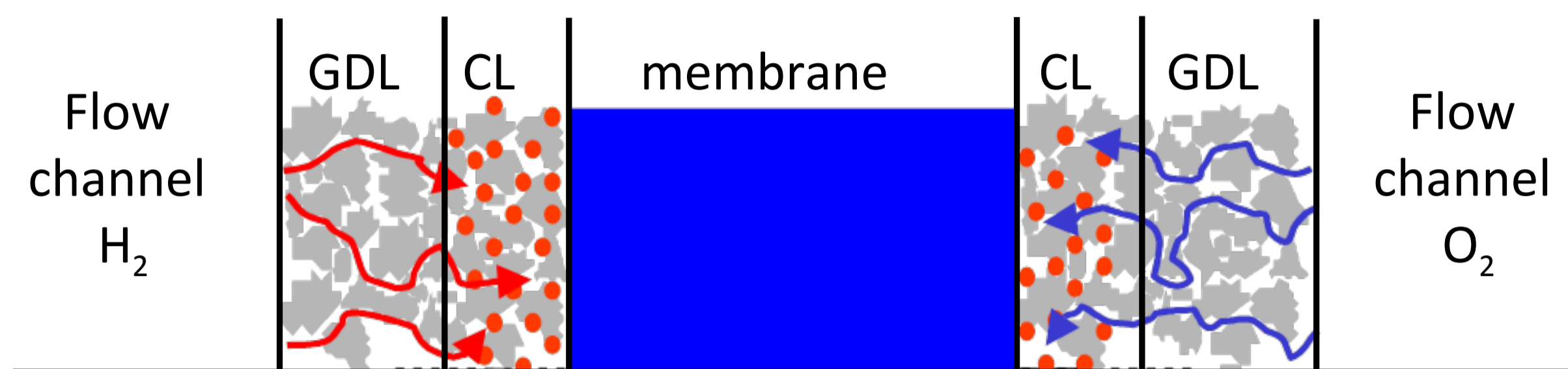


Figure 1. Multiphysics processes in PEM fuel cell.

Our approach to the problem was to get pressure values from the first model (gas distribution channels and porous layer) and then use these responses as initial values to simulate the second model (electrodes and membrane). The experimental tests of a prototype of a 144 cm² unitary fuel cell were carried out and the numerical model was validated.

Computational Methods:

Five reference channels were chosen to represent the Entire Plate model (Figure 2). These channels allow sampling of pressure and it was tabulated as initial values in MEA model (Figure 3). In the first model, Free and Porous Media Flow and Brinkman Equations were implemented in the flow channels and the GDL, as:

$$\rho \frac{\partial \mathbf{u}}{\partial t} - \nabla \eta (\nabla \mathbf{u} + [\nabla \mathbf{u}]^t) + \rho (\mathbf{u} \cdot \nabla) \mathbf{u} + \nabla p = 0$$

$$\nabla \cdot \mathbf{u} = 0$$

$$\rho \frac{\partial \mathbf{u}}{\partial t} - \eta \Delta \mathbf{u} + \frac{\eta}{k_p} \mathbf{u} + \nabla p = 0$$

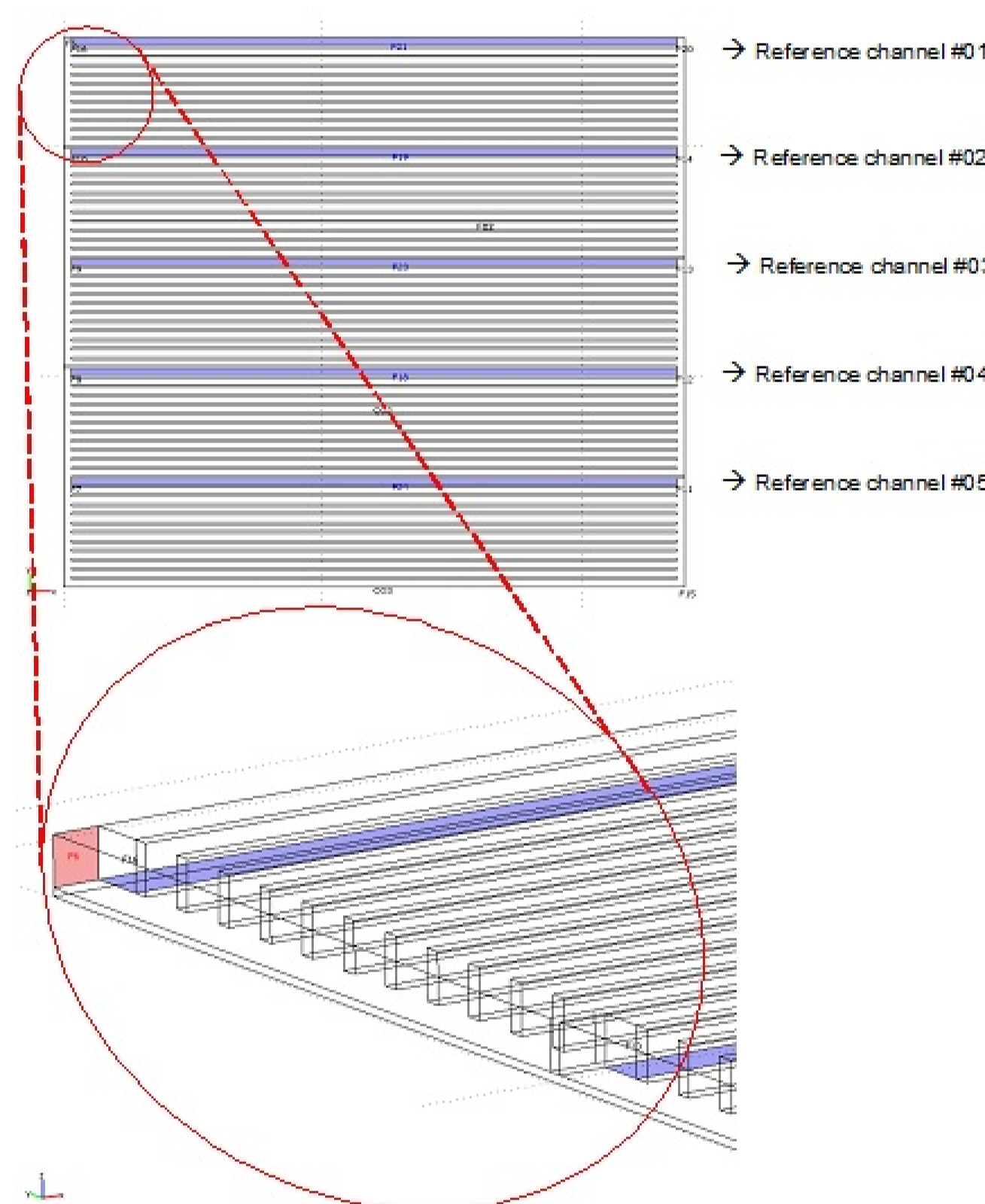


Figure 2. Reference channels.

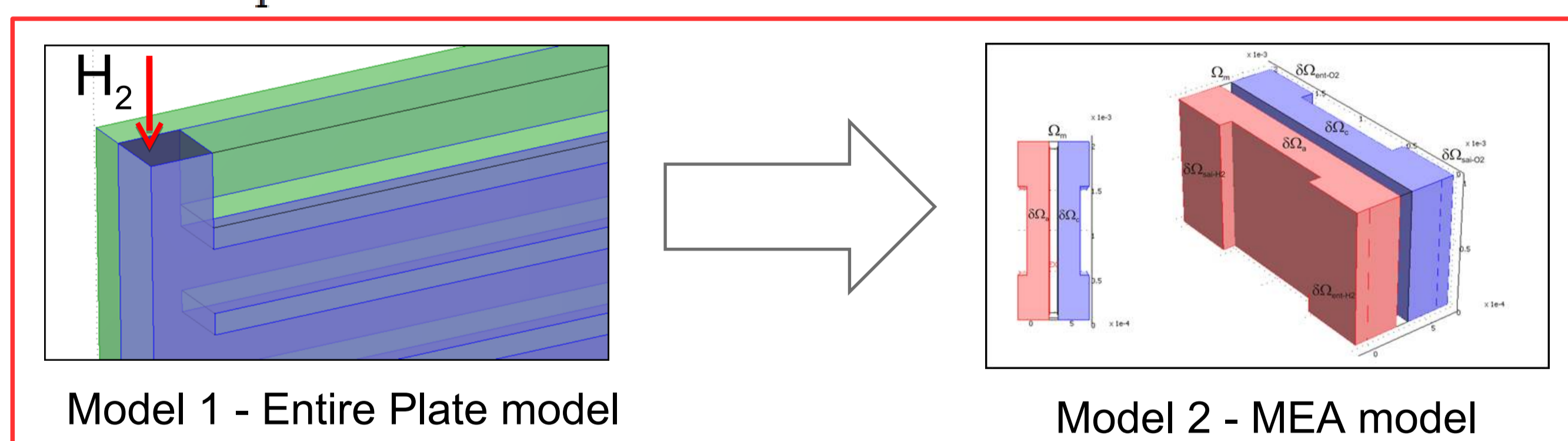


Figure 3. Coupling of models.

Secondary Current Distribution interface was applied in the MEA model, which contains of Butler-Volmer, Tafel and Ohm's equations. The electrochemical reactions, mass conservation as well as the idea of agglomerate in the catalyst layers and charge transport in membrane were implemented in the second model (Figure 4).

Maxwell-Stefan

$$\mathbf{n} \cdot \nabla \left[-\rho \omega_i \sum_{j=1}^N D_{ij} \left(\frac{M_j}{M} (\nabla \omega_j + \omega_j \frac{\nabla M}{M}) + (x_j - \omega_j) \frac{\nabla p}{p} \right) + D_i^* \frac{\nabla T}{T} + \rho \mathbf{u} \omega_i \right] = i_i$$

Laplace

$$\nabla \cdot [-k_e \nabla \phi_e] = 0 \text{ in } \Omega_a$$

$$\nabla \cdot [-k_m \nabla \phi_m] = 0 \text{ in } \Omega_m$$

$$\nabla \cdot [-k_e \nabla \phi_e] = 0 \text{ in } \Omega_c$$

B.C.

$$(-k_e \nabla \phi_e) \cdot \mathbf{n} = i_e \text{ in } \partial \Omega_a$$

$$(-k_e \nabla \phi_e) \cdot \mathbf{n} = i_c \text{ in } \partial \Omega_c$$

$$(-k_m \nabla \phi_m) \cdot \mathbf{n} = -i_e \text{ in } \partial \Omega_a$$

$$(-k_m \nabla \phi_m) \cdot \mathbf{n} = -i_c \text{ in } \partial \Omega_c$$

Mass flux

$$-\mathbf{n} \cdot \mathcal{S}_{H_2} = \frac{i_e}{2F} \text{ in } \partial \Omega_a$$

$$-\mathbf{n} \cdot \mathcal{S}_{O_2} = \frac{i_c}{4F} \text{ in } \partial \Omega_c$$

$$-\mathbf{n} \cdot \mathcal{S}_{H_2O} = \frac{drag}{F} \text{ in } \partial \Omega_a$$

Figure 4. Mathematical coupling of models.

Results: Numerical results of anode and cathode mass fractions, current density, pressure, velocity and convergence graphics were generated in the COMSOL Multiphysics® software. The polarization planes generated from MEA model are showed in Figure 5, highlighting the potential dependence of current density at cathode collector. These readings were obtained from the interface electrode-membrane, at T=348K (75°C), pref=1 atm, pH₂=pO₂= 52.45 Pa, 0<E(V)<1.0. In Figure 6 one can observe the non-uniform distributions of ionic current density in the middle plane of the membrane.

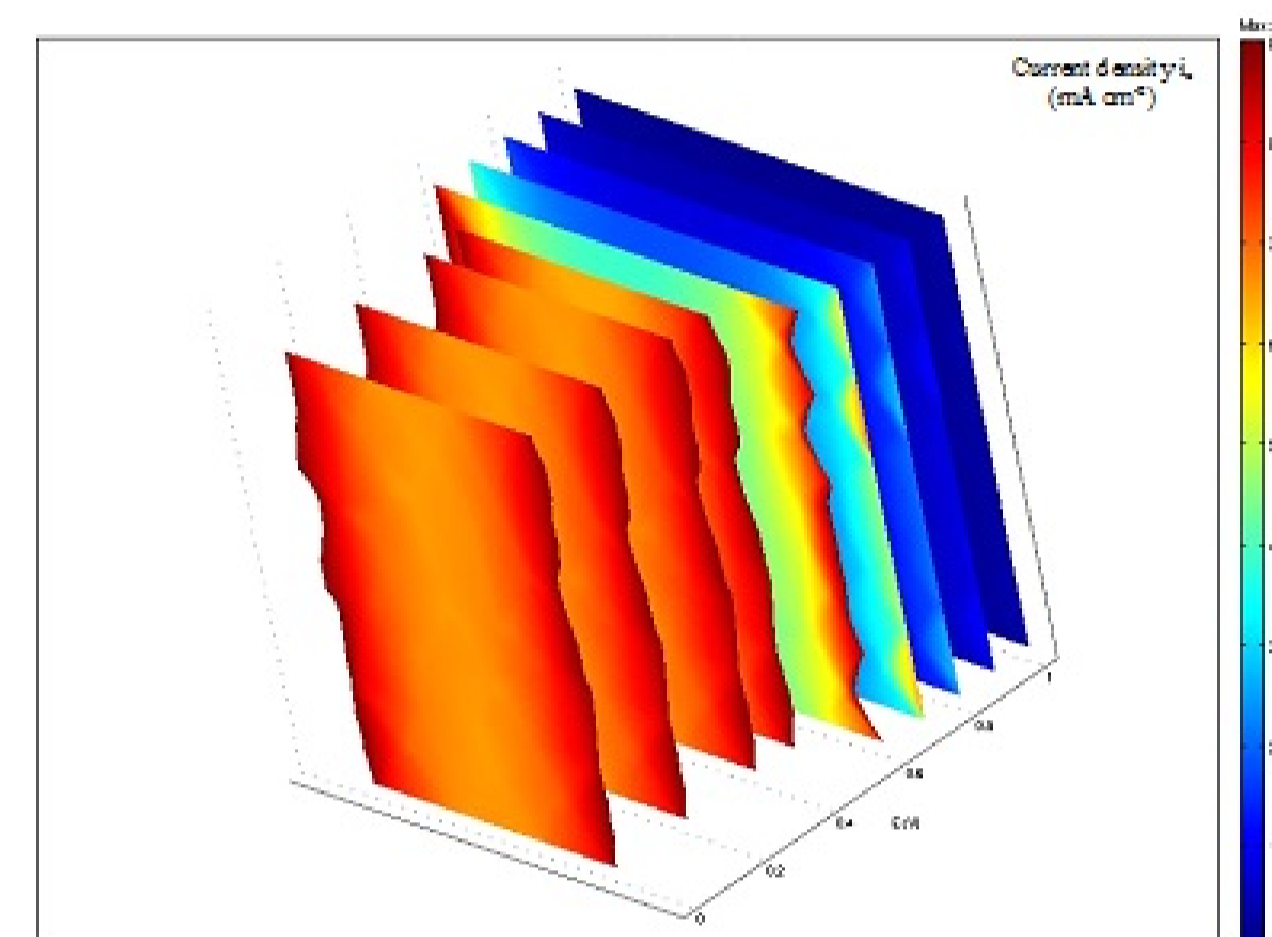


Figure 5. Polarization planes.

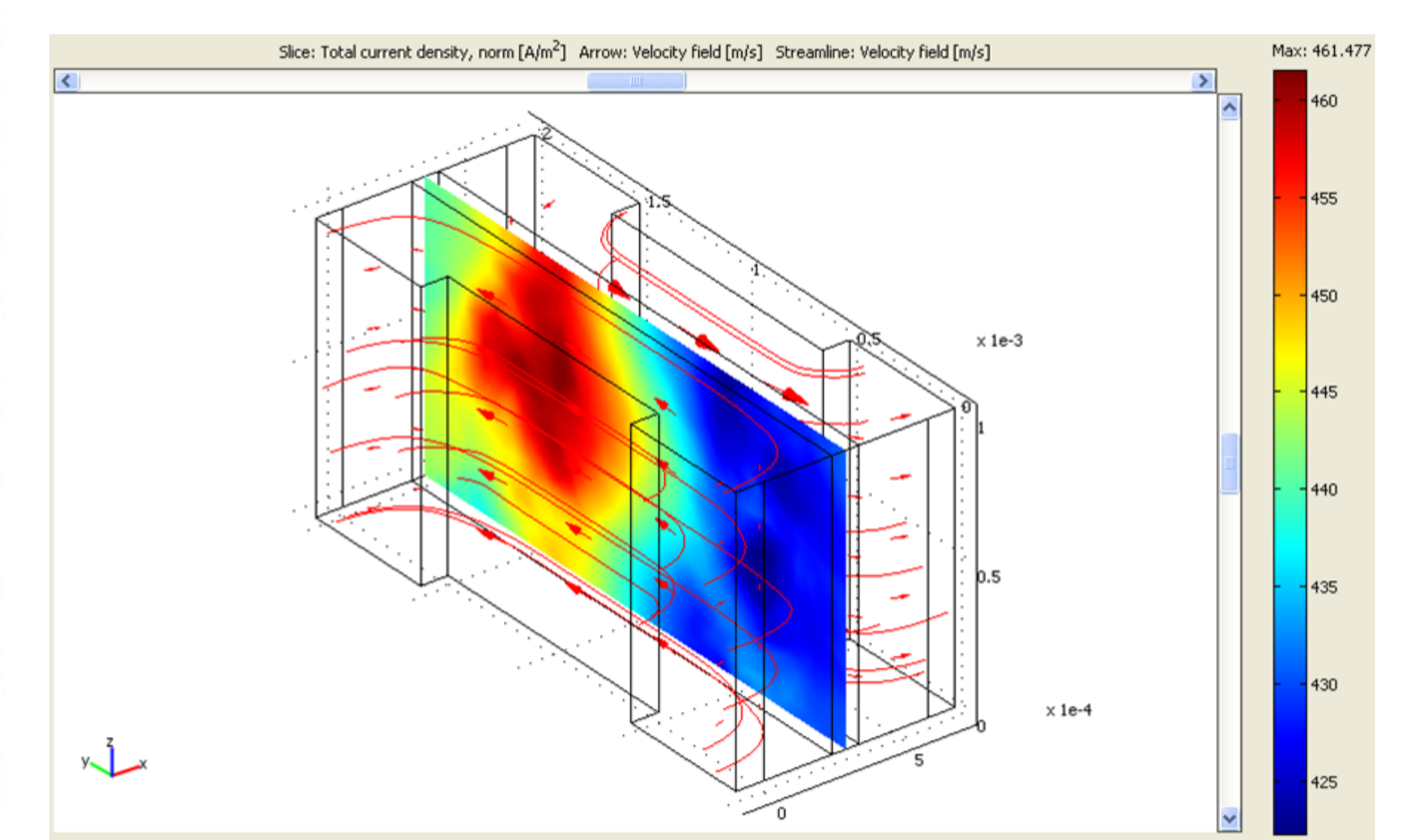


Figure 6. Ionic current density.

Polarization curves are showed in Figure 7, presenting numerical and experimental (MEA 02) responses. These are simulations results for the fuel cell operating under temperatures in the range of 293 K – 363 K (20 °C – 90 °C). Polarization curves were simulated, also, for pH₂ = 2 x pH₂, for each operating temperature, in order to check the numerical responses. The numerical simulations are comparable, but best fit was 348 K (75 °C).

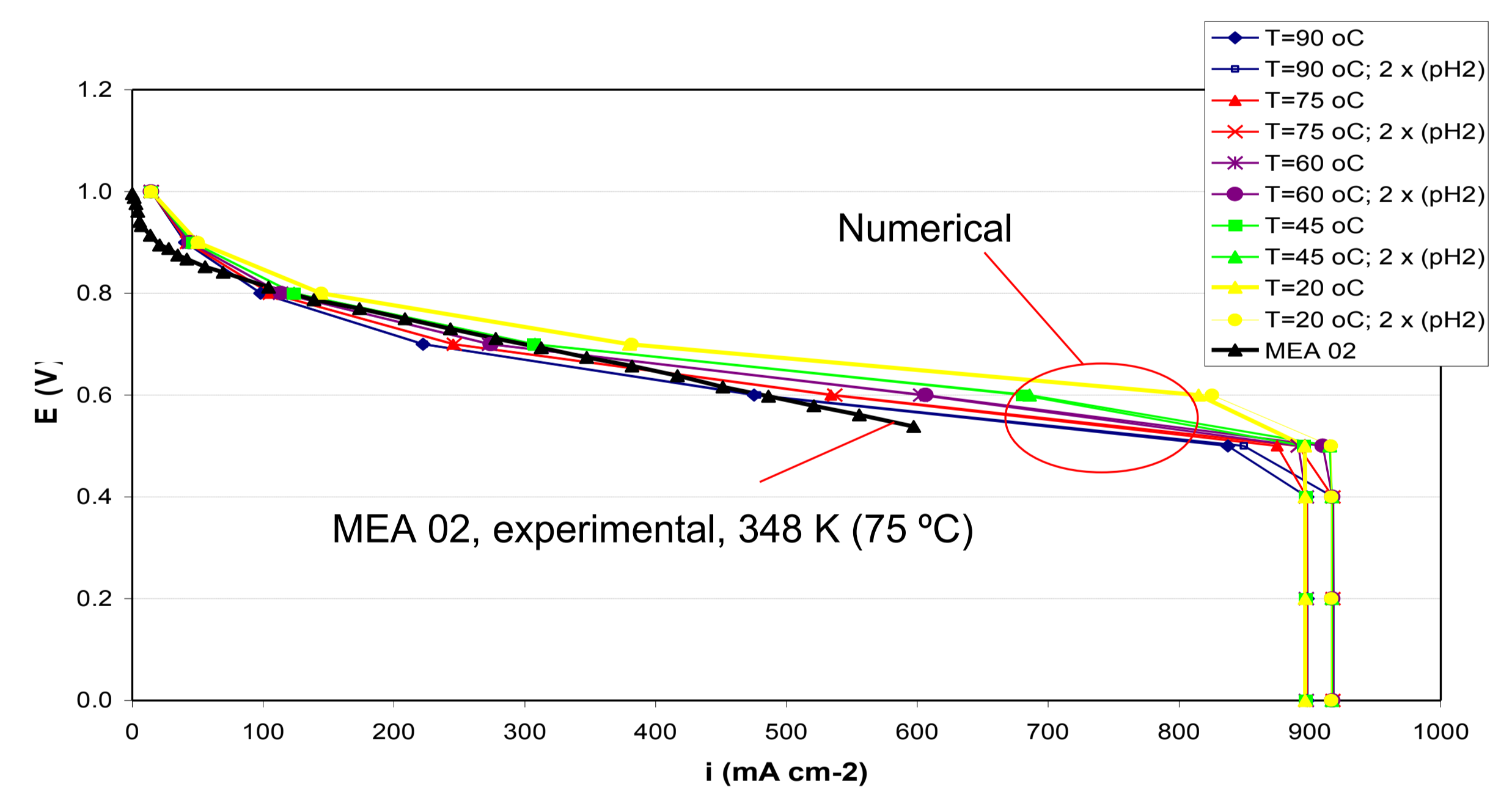


Figure 7. Polarization curves.

Conclusions: The strategy of coupling two 3D models satisfy the requirements of the comprehensive model of a unitary Proton Exchange Membrane fuel cell, including its internal geometries and constitutive materials, as well as distinct physical and chemical processes was successfully performed. The final model is robust and useful as a tool for design and optimization of PEM fuel cells in a wide range of operating conditions.

Acknowledgments:



References

- M. Linardi, Introdução à Ciência e Tecnologia de Células a Combustível, São Paulo, Artliber, (2010).
- J. Zhang, PEM Fuel Cell Electrocatalysts and Catalyst Layers: Fundamentals and Applications, Springer-Verlag London Limited, (2008).
- T.E. Springer; I.D. Raistrick, J. Electrochem. Soc. Electrical Impedance of a Pore Wall for the Flooded-Agglomerate Model of Porous Gas-Diffusion Electrodes. vol. 136, 1594-1603 (1989).
- K. Broka, Characterization of the Components of the Proton Exchange Membrane Fuel Cell, Techn. Lic. Thesis, Royal Institute of Technology, Stockholm, (1995).